J Water Environ Nanotechnol 2026, 11(3): 431-446
10.22090/jwent.2025.2071386.1966

RESEARCH PAPER

Hydrothermal Synthesis of ZnO/BiOCl/RGO Heterostructure: Characterization, Antibacterial Potential and Photocatalytic Removal of Tetracycline Antibiotic

Shobha Musmade[1], Shailendra Gurav[2], Kailas Kadam[1], Pranjali Badiger[3], Prashant Harale[1], Dinesh Hase[4], Vaishali Murade[1]**

[1]Department of Chemistry, Padmashri Vikhe Patil College of Arts Science and Commerce, Pravaranagar (Affiliated to Savitribai Phule Pune University, Pune), Ahilyanagar-413736, India
[2]Department of Pharmacognosy, Goa College of Pharmacy, Panaji, Goa University, Goa-403001, India
[3]Department of Microbiology, Rayat Shikshan Sanstha, S. M. Joshi College, Hadapsar, Pune-411028, India
[4]Department of Pharmacognosy, Amrutvahini College of Pharmacy (An Autonomous College), Sangamner, Ahilyanagar-422608, India

*Corresponding Author(s)
Email:
dinesh23787@gmail.com
vaishali.hase66@gmail.com

Article History:
Received: 2025-09-11
Revised: 2025-12-08
Accepted: 2025-12-16

How to cite this article
Musmade S, Gurav S, Kadam K, Badiger P, Harale P, Hase D, Murade V. Hydrothermal Synthesis of ZnO/BiOCl/RGO Heterostructure: Characterization, Antibacterial Potential and Photocatalytic Removal of Tetracycline Antibiotic. J Water Environ Nanotechnol 2026, 11(3): 431-446, DOI: 10.22090/jwent.2025.2071386.1966

HIGHLIGHTS

- Synthesis of ternary ZnO/BiOCl/RGO heterostructure by hydrothermal method with the ability to absorb visible radiation.
- ZnO/BiOCl/RGO heterostructure was elucidated by various characterization techniques.
- Photocatalytic efficiency (85.95% in 80 min.) was tested with tetracycline antibiotic under UV-visible radiation.
- Antibacterial potential was evaluated against multiple drug-resistant bacteria, namely Gram-positive S. aureus (NCIM 2654) and Gram-negative E. coli (NCIM 2256).

ABSTRACT

Antibiotics are one of the primary contaminants found in wastewater released by the pharmaceutical industry, and they are harmful to both humans and aquatic life. It is essential to eliminate these contaminants from water bodies using an economical yet efficient technique. The goal of the current work is to create affordable nanomaterials for the removal of tetracycline (TC) antibiotic from wastewater as well as to inhibit the growth of Gram-positive (*S. aureus*) and Gram-negative (*E.coli*) bacteria. The ZnO/BiOCl/RGO heterostructure was produced using a simple hydrothermal method, and its synthesis, structure, metal-oxygen and functional group vibrations, morphology, elemental composition, and optical absorption properties were subsequently confirmed through XRD, FT-IR, SEM, EDX, TEM, XPS, and UV-vis DRS techniques. The synthesized heterostructure was tested for the catalytic degradation of TC antibiotic, and it showed 85.95 % removal in 80 minutes. Antibacterial potential of the heterostructure was evaluated against multiple drug-resistant bacteria. The synthesized ZnO/BiOCl/RGO exhibited a strong zone of inhibition against both bacterial strains stated here. The findings of this study strongly support the application of the synthesized heterostructure in wastewater treatment, particularly for the elimination of antibiotics and microorganisms.

KEYWORDS:

Antibacterial Activity; Tetracycline; Photocatalytic Degradation; Water Pollution.

©2026 The Author(s). Published by the Iranian Environmental Mutagen Society. This work is licensed under the Creative Commons Attribution 4.0 International License (CC BY 4.0). To view a copy of this license, visit http://creativecommons.org/licenses/by/4.0/.

1. INTRODUCTION

Pharmaceutical antibiotics like Tetracycline (TC) have sparked a lot of attention because of their slow metabolism, excellent chemical stability, and high water solubility, which can lead to significant water contamination [1]. The aquatic ecosystem and human health are significantly jeopardised by these toxins, which can result in severe issues such as chronic toxicity and antibiotic resistance, even at minimal quantities. As a result, remediation of these pollutants from wastewater is very necessary. These hazardous pollutants have been removed from water using several methods, including flocculation [2], adsorption [3], chlorination [4], and biodegradation [5]. Although these approaches demonstrate a certain level of effectiveness, they are hindered by multiple limitations, such as the creation of byproducts, steep expenses, lengthy processes, and insufficient eradication. To tackle these challenges, innovative oxidation methodologies (IOMs), which harness the power of reactive oxygen entities to eradicate contaminants, have captured heightened fascination [6]. Due to the outstanding performance and direct use of solar energy, photocatalyst-based semiconductors are the most effective method for wastewater treatment [7-12].

As an n-type semiconductor (E_g = 3.2 eV), Zinc oxide (ZnO) has superior organic pollutant breakdown efficiency, enhanced photosensitivity, and faster electron mobility [13]. However, its photocatalytic activity is limited by inadequate solar spectrum absorption and rapid recombination of photoexcited electrons (e^-) and holes (h^+). Therefore, combining it with p-type semiconductors could be the best alternative to resolve the stated limitations [14]. The coupled n-p type heterojunction shows superior photocatalytic efficiency compared to its pristine components. Their photocatalytic effectiveness is increased through improved charge carrier separation and full solar spectrum utilization [15]. Bismuth oxyhalides (BiOX; where X = Cl, Br, I) are widely used photocatalysts among several bismuth-based semiconductors because of their distinct layered structure and outstanding photostability [16,17]. However, BiOCl consists of [Cl-Bi-O-Bi-Cl] layered sheets. The internal electric field between $[Bi_2O_3]^{2+}$ and chloride ions (Cl^-) improves photocatalytic degradation performance by increasing e^-/h^+ pair separation [18]. The BiOCl/ZnO heterojunction exhibited an exceptional degrading ability towards TC-HCl compared to pure ZnO and BiOCl nanoparticles [19]. Similarly, Yang and colleagues found that the photodegradation was significantly enhanced by strong BiOCl/ZnO heterostructure formation [20]. The heterojunctions between these two catalysts reduce e^-/h^+ pair recombination, thereby improving photocatalytic degradation efficacy.

Reduced graphene oxide (RGO) is a 2D graphitic material and consists of a sp^2 hybridized network of hexagons [21,22]. Its excellent stability, high electrical conductivity, robust electron transport, and broad surface area make it an efficient photocatalytic material. Additionally, RGO has a 2000 mg/g adsorption capability; thus, it serves as an excellent example of a pollutant adsorbent. On the RGO surface, the organic contaminants are adsorbed through electrostatic, van der Waals, hydrogen bonding, and π-π interactions. [23]. RGO, combined with semiconductor oxides, has attracted enormous attention as it enhances photo-driven reactions by separating the photogenerated e^-/h^+ pair of photocatalysts at the catalyst/RGO interface [24,25]. Thus, developing a ZnO/BiOCl heterojunction photocatalyst based on reduced graphene oxide is crucial today.

This study's novelty is the synthesis of the ZnO/BiOCl@RGO heterostructure by a straightforward hydrothermal process and its application in the photodegradation of TC. This study addresses the specific problem of antibiotic concentration utilising ZnO/BiOCl@RGO, in contrast to previous research that investigated several nanocomposites for the breakdown of organic contaminants. Employing the hydrothermal approach, we achieved a homogeneous composite structure characterised by enhanced purity, increased surface area, superior catalytic activity, and reduced photoexcited charge recombination. The loading quantities of ZnO/BiOCl@RGO and pH were crucial in attaining an exceptional photodegradation rate of TC (85.95%) within 80 minutes, surpassing previous research [26,27]. The ZnO/BiOCl@RGO heterostructures, characterised by remarkable stability, robust light absorption, and enhanced photocatalytic performance, present a compelling solution for the remediation of various pollutants beyond TC, including other antibiotics, dyes, and organic pollutants. Our previous study [13] successfully reported a novel S-scheme ternary photocatalyst as a cost-efficient solution for the remediation of contaminated water by degrading the carcinogenic dyes (Methylene blue and Malachite green) in industrial effluents. In view of its photocatalytic potential, the present research reports a ternary ZnO/BiOCl/RGO heterostructure synthesis by a simple, one-pot hydrothermal method, physicochemical characterization, and, for the first time, the photocatalytic breakdown of TC, along with its antibacterial potential against multiple drug-resistant bacteria, namely *S. aureus* (NCIM 2654) and *E. coli* (NCIM 2256).

2. MATERIALS AND METHODS

2.1. Materials

Sodium hydroxide (NaOH, 97%, MW:40), zinc acetate dihydrate ($Zn(CH_3COO)_2.2H_2O$, 98%, MW:219.51), potassium chloride (KCl, MW:74.15), and bismuth nitrate pentahydrate ($Bi(NO_3)_3.5H_2O$, 99.5% MW:485.07) were obtained from Merck chemicals, India and the Hydrochlordie salt of TC ($C_{22}H_{25}N_2O_8Cl$, 88% purity, MW: 444.43) was procured from Sigma Aldrich and RGO was acquired from Techinstro Industries, India.

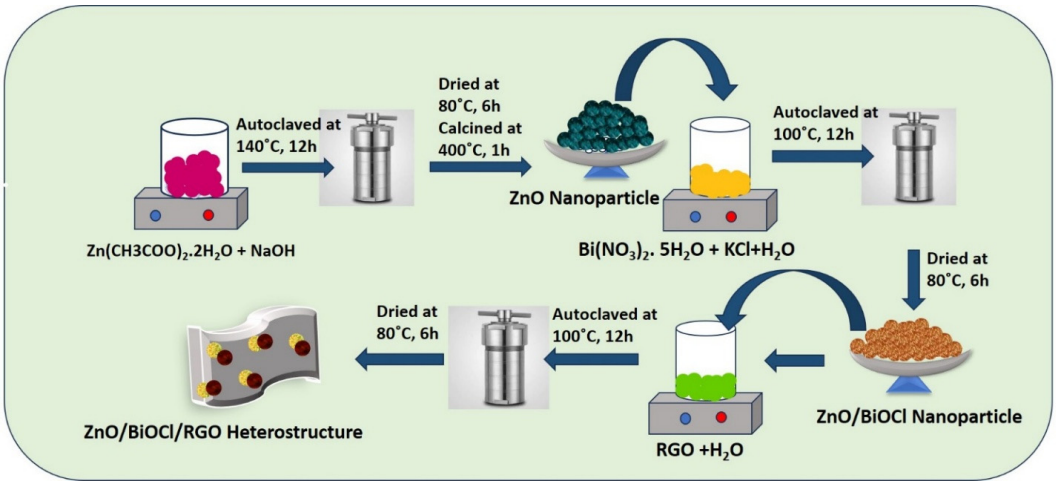

Fig. 1. Schematic illustration of synthesis of ternary ZnO/BiOCl/RGO heterostructure

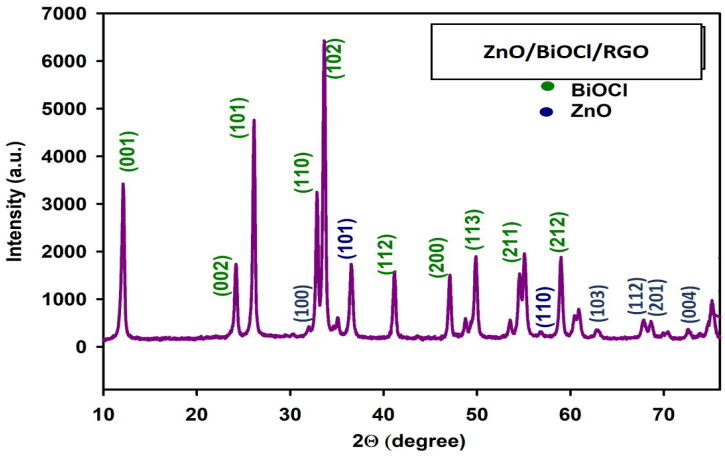

Fig. 2. X-ray diffraction pattern of ternary ZnO/BiOCl/RGO heterostructure.

2.2. Synthesis of ZnO nanoparticles (ZnONPs)

First, 1.371 g zinc acetate and 0.6 g NaOH were dissolved separately in 20 mL of deionized water, and the prepared solution was added slowly to the zinc acetate solution. For 12 h, the reaction mixture was autoclaved at 140°C. The precipitate was washed and dried for 6 h at 80°C after cooling to room temperature. ZnONPs were then obtained by calcining the product for one hour at 400°C [16].

2.3. Synthesis of binary ZnO/BiOCl composite

Briefly, 40 mL of deionised water was used to dissolve 0.25 g of KCl and 1.616 g of $Bi(NO_3)_3.5H_2O$. The aforementioned combination was then supplemented with 0.405 g of synthesised ZnONPs. The solution was then autoclaved for 12 h at 100°C. A binary ZnO/BiOCl composite was then produced by drying the resultant material for 6 h at 80ºC [16].

2.4. Synthesis of ternary ZnO/BiOCl/RGO heterostructure

Firstly, 50 mg of the BiOCl/ZnO composite solution in deionized water (80mL) was sonicated at RT for 20 min. 10 mg of RGO was added and stirred into the above-prepared solution for 1 h at RT. The resultant mixture was then autoclaved at 100ºC for 12 h. Ultimately, the precipitate was cleaned multiple times using deionised water, dried for 6 h at 80ºC, and then utilised for further research. Fig. 1 shows the ternary ZnO/BiOCl/RGO heterostructure synthesis schematic design.

2.5. Antibacterial Assay

The well diffusion method was used to assess the antibacterial activity of synthesised ZnO, ZnO/BiOCl, and ZnO/BiOCl/RGO NPs at a concentration of 2 mg/mL against several drug-resistant bacteria, specifically *S. aureus* and *E. coli*. The

J Water Environ Nanotechnol, 2026, 11(3): 431-446
10.22090/jwent.2025.2071386.1966

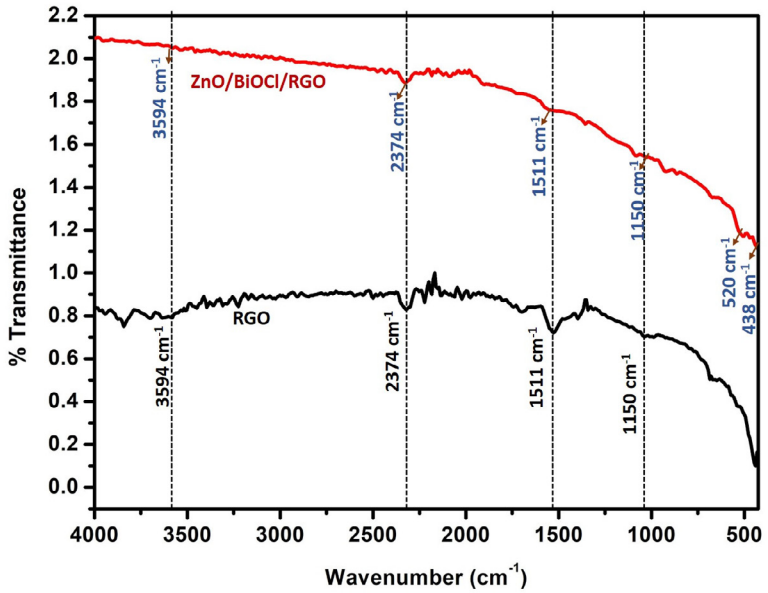

Fig. 3. FT-IR spectra of pure RGO and ternary ZnO/BiOCl/RGO heterostructure

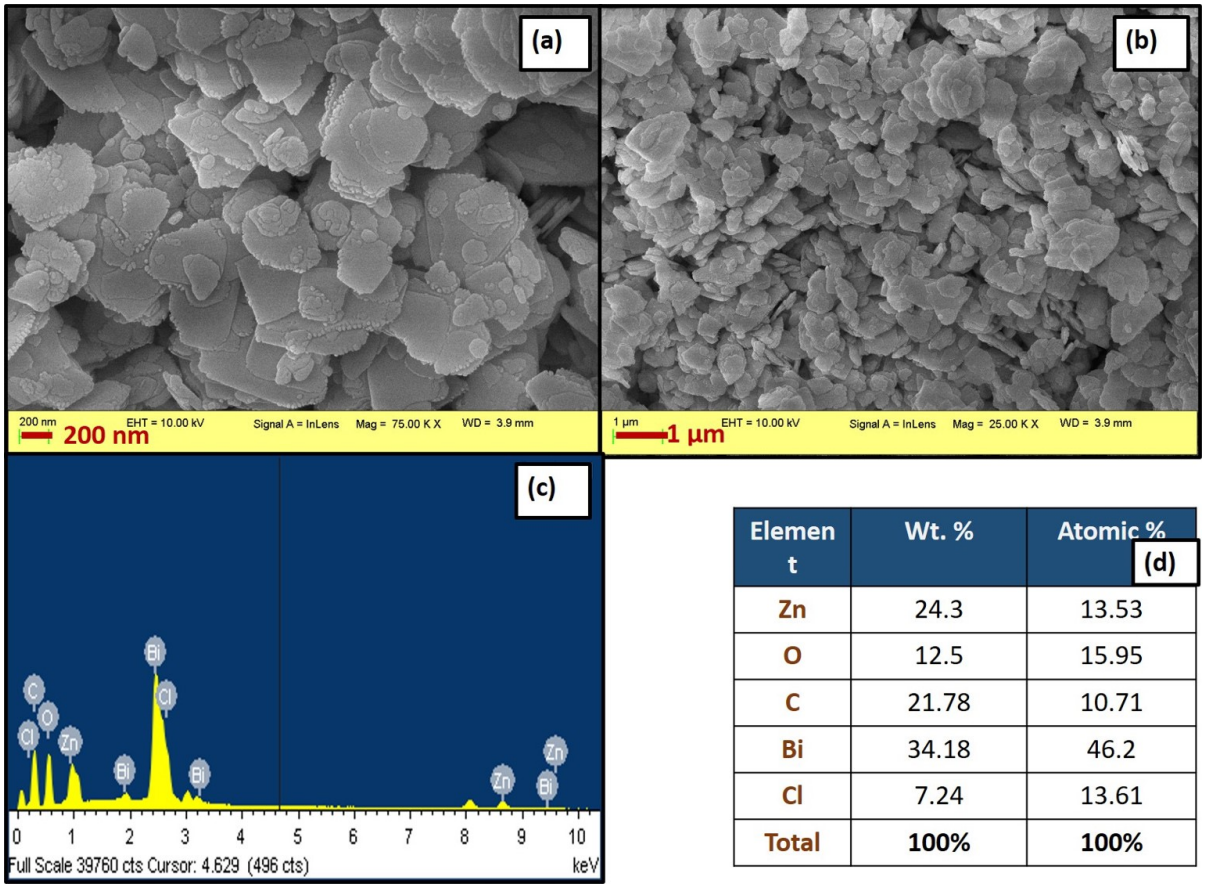

Element	Wt. %	Atomic %
Zn	24.3	13.53
O	12.5	15.95
C	21.78	10.71
Bi	34.18	46.2
Cl	7.24	13.61
Total	**100%**	**100%**

(d)

Fig. 4. FESEM micrographs (a,b) and EDX (c,d) analysis of ZnO/BiOCl/RGO heterostructure.

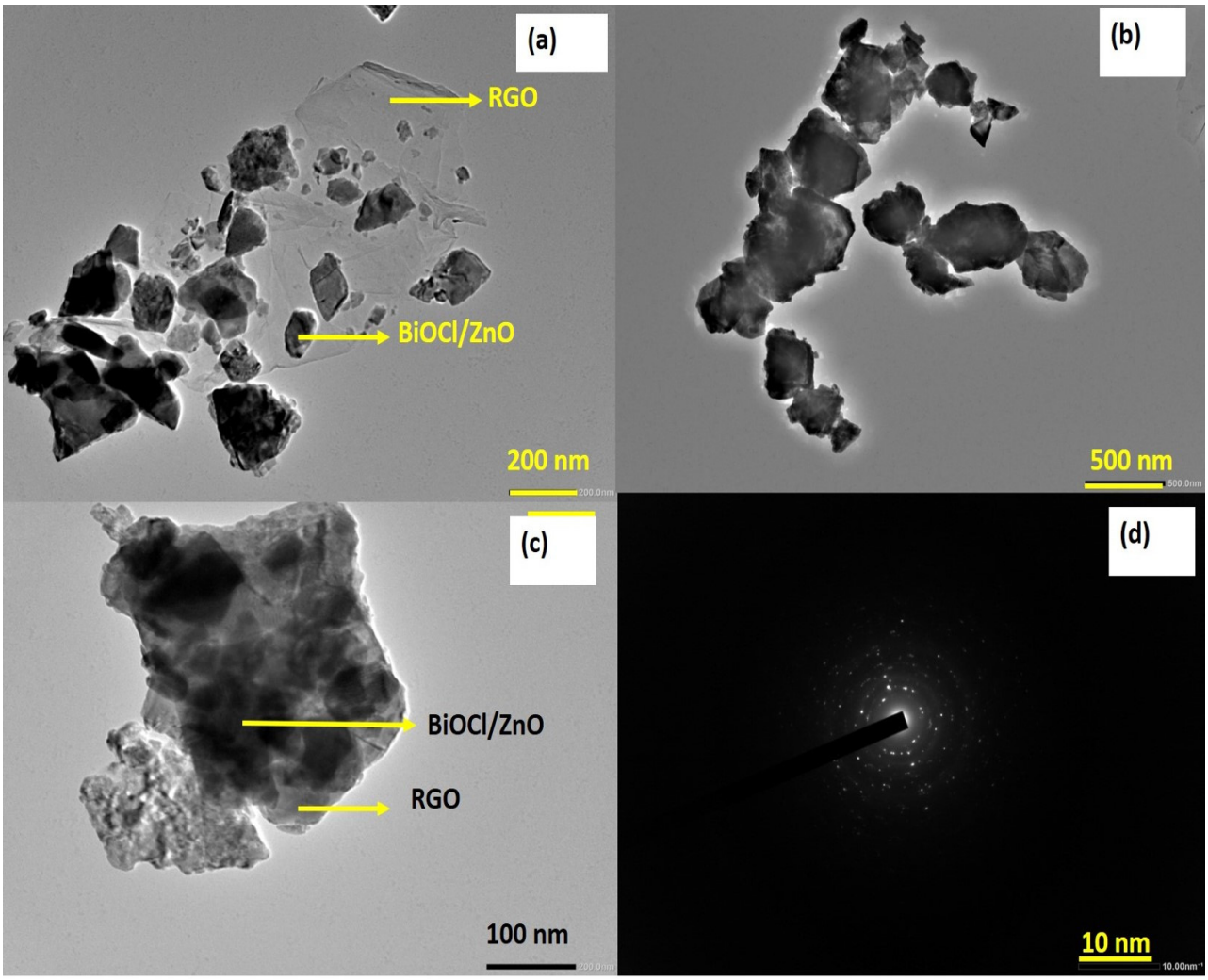

Fig. 5. TEM pictures (a-c) and selected area electron diffraction pattern (d) of the ZnO/BiOCl/RGO heterostructure.

resulting suspensions of bacteria were diluted to a final OD at 600nm of 0.02 using UV-visible, i.e $2*10^7$ CFU. Under aseptic conditions, wells were shaped on the sterile nutrient agar plate, and the 50 µL sample was added to each well. The diameter of the inhibition zones during a 24 h incubation period at 37°C was used to assess the antibacterial activity [28,29].

2.6. Photocatalytic degradation study

TC was degraded photocatalytically at room temperature. Here, 50 mL of deionised water was used to dissolve 10 mg of TC, and 30 mg of the produced catalyst were then added to the mixture. Magnetic stirring was used at room temperature to agitate the resulting reaction mixture to adsorb TC onto the catalyst surface. The mixture was exposed to visible light radiation using a 250W xenon lamp to further start the catalytic reaction. After centrifuging 5 mL of the reaction mixture at regular intervals, the absorbance at λ=379 nm was measured using a UV-visible spectrophotometer. Furthermore, the photocatalytic degradation efficacy (%) of TC was calculated using the following formula [13];

Degradation efficiency (%) = $(C_0\text{-}C_t/C_0) \times 100$;

where C_0 and C_t are initial and final concentrations.

2.7. Characterization of synthesized nanomaterial

X-Ray Diffraction (XRD) analysis (Mini Flex 600 X-ray diffractometer) was performed to explore the crystal structure of the ternary ZnO/BiOCl/RGO heterostructure. The FT-IR spectra were recorded on a Bruker Optics Alpha-T FT-IR spectrometer. FESEM (Hitachi SU8010 Series, Japan) equipped with an energy dispersive spectrometer (EDS), and HR-TEM (JEOL, JEM 2100 Plus) analysis were utilized to explore the surface and structural morphology of the catalyst. To explore the elemental oxidation states and binding energies

J Water Environ Nanotechnol, 2026, 11(3): 431-446
10.22090/jwent.2025.2071386.1966

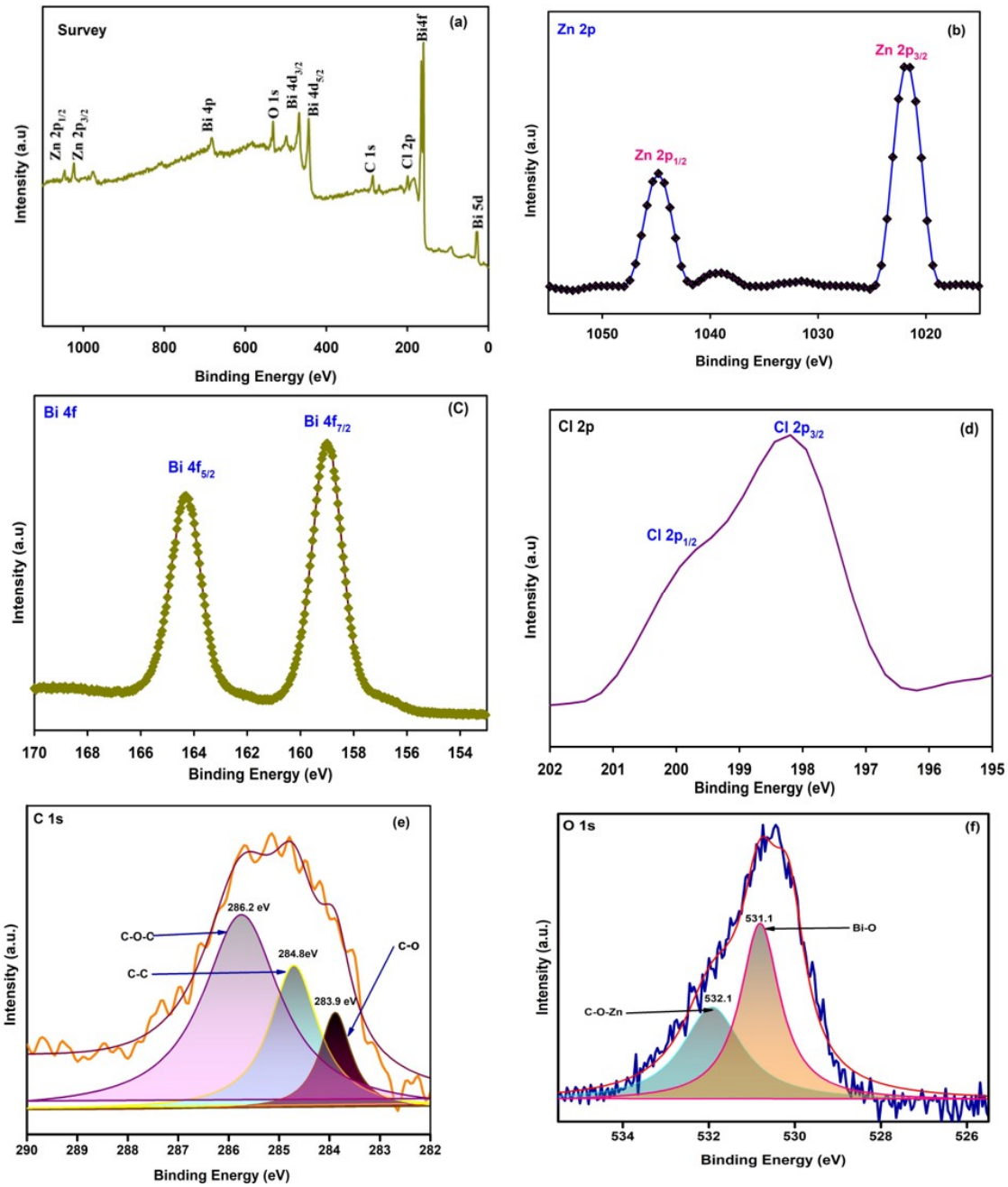

Fig. 6. XPS survey spectrum (a), high-resolution spectra of zinc (b), bismuth (c), chlorine (d), carbon (e), and oxygen (f) elements of ZnO/BiOCl/RGO heterostructure

of the different bonds in the prepared catalyst, XPS (Physical Electronics, PHI 5000 Versa Probe III) analysis was performed. UV-visible DRS spectrophotometer (Shimadzu, UV 2600) was used to investigate the band gap energies of the prepared catalysts. The UV–visible absorption spectra of TC were measured on a UV-visible spectrophotometer (Systronics, UV 2202).

3 RESULTS AND DISCUSSION

3.1. Powder XRD analysis

A Mini Flex 600 X-ray diffractometer was used for the XRD investigation to investigate the crystalline phases found in the ZnO/BiOCl/RGO heterostructure. The obtained XRD patterns are displayed in Fig. 2. The diffraction peaks at 31.78°,

36.26°, 56.58°, 62.84°, 67.94°, 68.99°, and 72.57° correspond to (100), (101), (110), (103), (112), (201), and (004) diffraction planes of hexagonal phase of zinc oxide (JCPDS No. 36-1451) [30]. However, the BiOCl show the diffraction peaks at 12.05°, 24.07°, 25.87°, 32.56°, 33.47°, 40.84°, 46.78°, 49.82°, 54.12°, and 58.74° correspond to (001), (002), (101), (110), (102), (112), (200), (113), (211), and (212) diffraction planes of tetragonal phase of bismuth oxychloride (JCPDS No. 06-0249) [31,32]. However, because of the extremely amorphous nature and extremely low content, the diffraction peaks for RGO were not apparent in the XRD pattern [33]. The developed ZnO/BiOCl/RGO heterostructure is purer, as seen by the lack of additional peaks in the XRD pattern.

3.2. FT-IR analysis

The FT-IR technique is used to study the structural characteristics of the functional groups of RGO and ZnO/BiOCl/RGO nanocomposite; the spectra are shown in Fig. 3. The FT-IR spectra of RGO exhibit peaks at 1150 cm^{-1}, 1511 cm^{-1}, 2374 cm^{-1}, and 3594 cm^{-1}, corresponding to the stretching of C-O, C=C (aromatic), C-H, and O-H bonds [34,35]. The ZnO/BiOCl/RGO composite exhibits IR stretching peaks at 438 cm^{-1} and 520 cm^{-1}, which correspond to Zn-O and Bi-O bonds, respectively. The vibrations at 1150 cm^{-1} corroborated the establishment of a chemical connection between reduced graphene oxide and the ZnO/BiOCl combination [36].

3.3. Structural and morphological analysis of ZnO/BiOCl/RGO heterostructure

FESEM analysis characterized the ternary ZnO/BiOCl/RGO heterostructure's morphology and structural characteristics; the resulting micrographs are displayed in Fig. 4. The ZnO/BiOCl/RGO heterostructure's SEM micrographs displayed an irregular shape resembling nanoplates. Magnified SEM micrographs also show the ZnO/BiOCl nanoplates' coarse surface and monodispersed structure, which suggests a broader specific surface area and more active sites for efficient photocatalytic breakdown of organic pollutants [37].

Energy-dispersive X-ray spectroscopy (EDX) examination also confirms the presence of zinc, bismuth, oxygen, and chlorine in the synthesized heterostructure (Fig. 4c-4d). However, each component is evenly distributed, indicating that the ZnO/BiOCl/RGO heterostructure has been successfully produced. Fig. 5 (a-c) displays TEM images of the ZnO/BiOCl/RGO heterostructure, demonstrating that the sample is composed of irregular plate-shaped structures that range in thickness from 40 nm to 55 nm. TEM images confirmed that the uneven ZnO/BiOCl composite plates are evenly distributed across the RGO surface.

Furthermore, the highly crystalline plates of the ZnO/BiOCl/RGO heterostructure are confirmed by the corresponding SAED pattern, depicted in Fig. 5d.

3.4. X-ray photoelectron spectroscopy analysis

XPS analysed the surface elemental composition and chemical oxidation state of the ZnO/BiOCl/RGO heterostructure (Fig. 6). The survey scan spectra validated the presence of zinc, bismuth, oxygen, chlorine, and carbon elements in the ZnO/BiOCl/RGO heterostructure (Fig. 6a). The high-resolution Zn 2p XPS spectrum (Fig. 6b) reveals two peaks at binding energies of 1044.8 eV and 1021.5 eV, corresponding to Zn $2p_{1/2}$ and Zn $2p_{3/2}$, respectively, indicating the presence of zinc in +2 oxidation state in the synthesized heterostructure [38]. Additionally, the Bi 4f spectra exhibit two prominent peaks at 159.1 and 164.2 eV, corresponding to Bi $4f_{7/2}$ and Bi $4f_{5/2}$ (Fig. 6c), confirming the presence of bismuth in the +3-oxidation

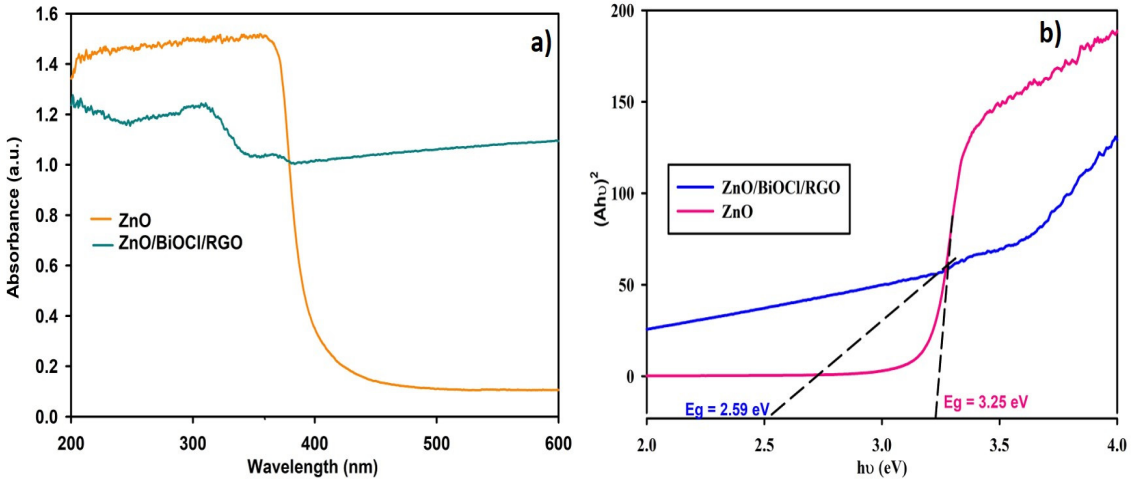

Fig. 7. UV-visible DRS spectra (a) and the Tauc plots (b) of ZnO/BiOCl/RGO heterostructure

J Water Environ Nanotechnol, 2026, 11(3): 431-446
10.22090/jwent.2025.2071386.1966

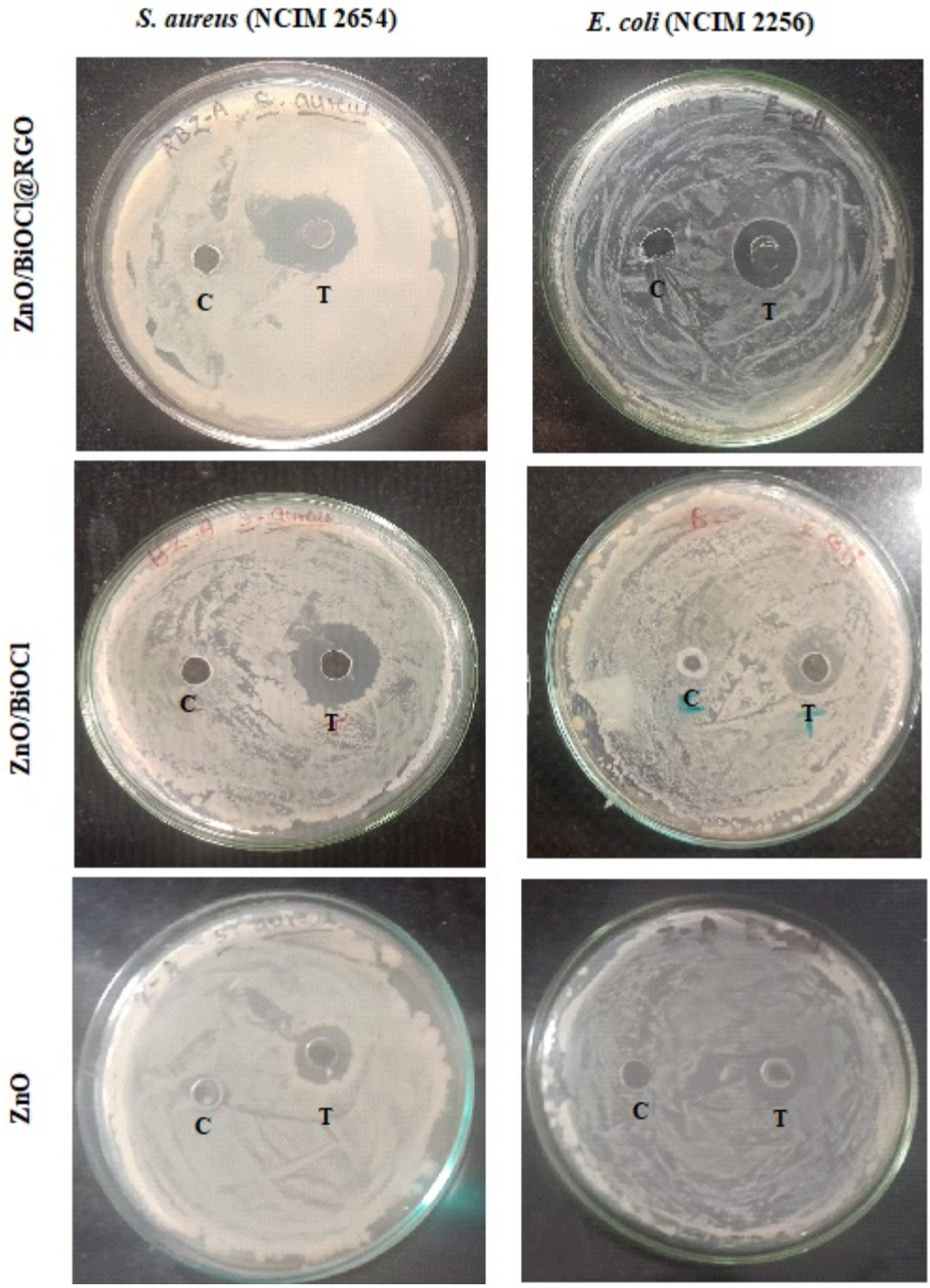

Fig. 8. Antibacterial activity of ZnO/BiOCl/RGO, ZnO/BiOCl, and ZnO against multiple drug-resistant bacteria *S. aureus* and *E. coli*

state within the ZnO/BiOCl/RGO heterostructure [39]. Furthermore, the Cl 2p spectra exhibited two peaks at 199.8 eV and 198.3 eV, corresponding to Cl $2p_{1/2}$ and Cl $2p_{3/2}$ of Cl^-, respectively (Fig. 6d) [14]. The XPS spectra of C 1s (Fig. 8e) exhibited three peaks: one at 283.8 eV, indicative of carbon-carbon single (C-C) bonds [40]; another at 284.7 eV, attributed to carbon-carbon double (C=C, Sp^2) bonds; and a peak at 286.1 eV, signifying C-O-C bonds in hydroxyl and epoxy groups, thereby confirming the presence of reduced graphene oxide [41].

Table 1. Results showing zones of inhibition against multiple drug-resistant bacteria *S. aureus* and *E. coli*

NPs/NCs	Zones of inhibition (mm)	
	S. aureus	*E. coli*
ZnO/BiOCl/RGO	7.23 ± 0.11	5.47 ± 0.55
ZnO/BiOCl	6.13 ± 0.25	4.27 ± 0.12
ZnO	5.06 ± 0.11	4.1 ± 0.20

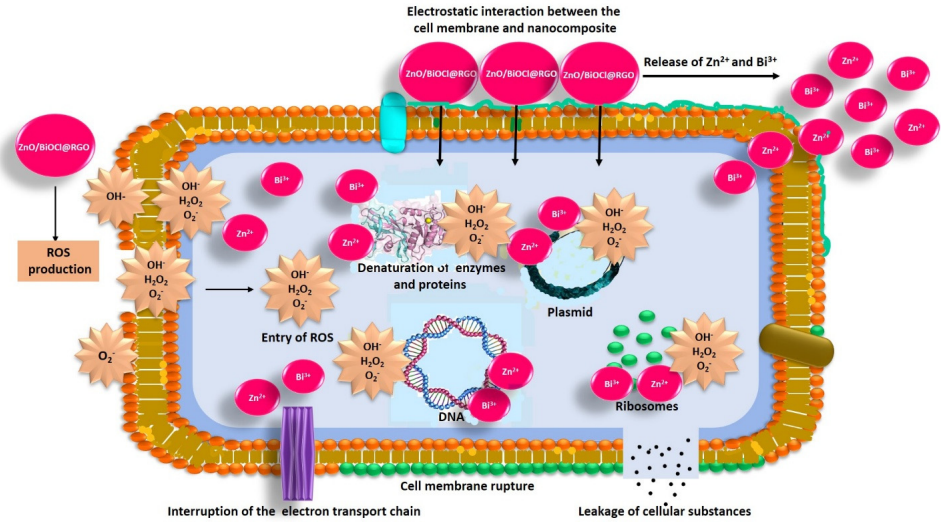

Fig. 9. Plausible antibacterial mechanism using ZnO/BiOCl/RGO heterostructure

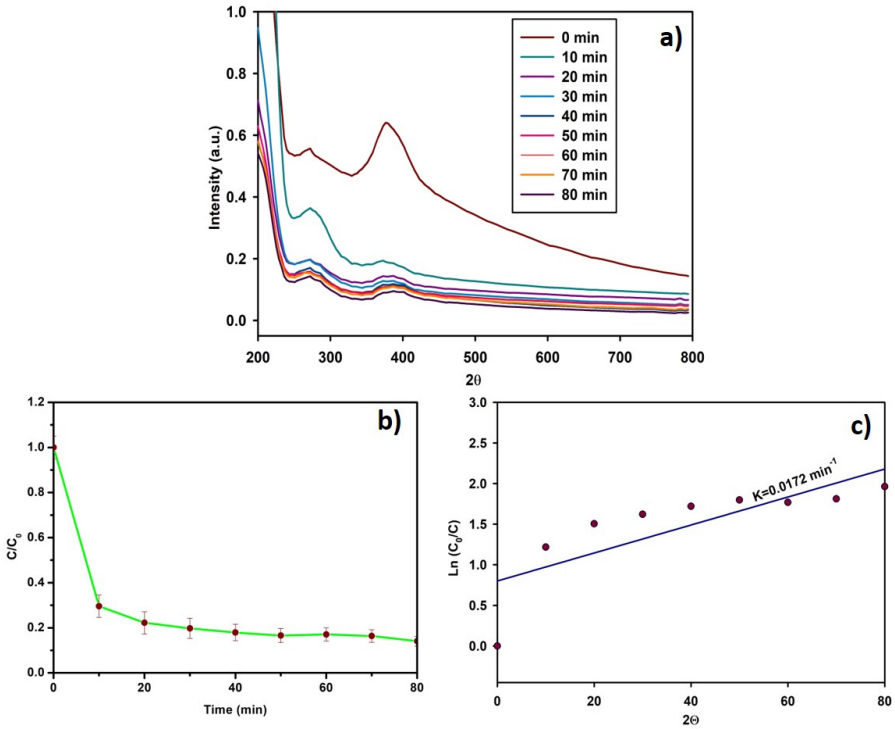

Fig. 10. UV-visible absorption spectra of TC degradation (a), and degradation plot of TC (b), pseudo-first-order kinetics plot for tetracycline degradation (c).

J Water Environ Nanotechnol, 2026, 11(3): 431-446
10.22090/jwent.2025.2071386.1966

Table 2. Comparison of TC degradation using ZnO/BiOCl/RGO heterostructure with previously reported nanocomposites.

Photocatalysts	Degradation Efficiency (%)	Degradation time (min)	Light source	References
Multiwalled carbon nanotubes/TiO_2	83.00	300	visible light	[41]
Black anatase TiO_2	66.20	270	UV light	[42]
RGO/Mn	85.2	180	Visible light	[43]
Maghemite	40	60	UV-visible	[44]
$Bi_2Fe_4O_9$/RGO	83.73	60	visible light	[45]
$BIVO_4$/α-Fe_2O_3	75.8	120	visible light	[46]
$CoFe_2O_4$/TiO_2	75.31	180	UV light	[47]
g-C_3N_4	84.60	40	sunlight	[48]
g-C_3N_4/Ag/AgBr	57.50	30	sunlight	[49]
Au-TiO_2	75	120	visible light	[59]
N-doped TiO_2	66.2	120	visible light	[60]
Fe_3O_4/g-C_3N_4/TiO_2	73.61	100	visible light	[61]
ZnO/BiOCl/RGO	85.95	80	visible light	Present work

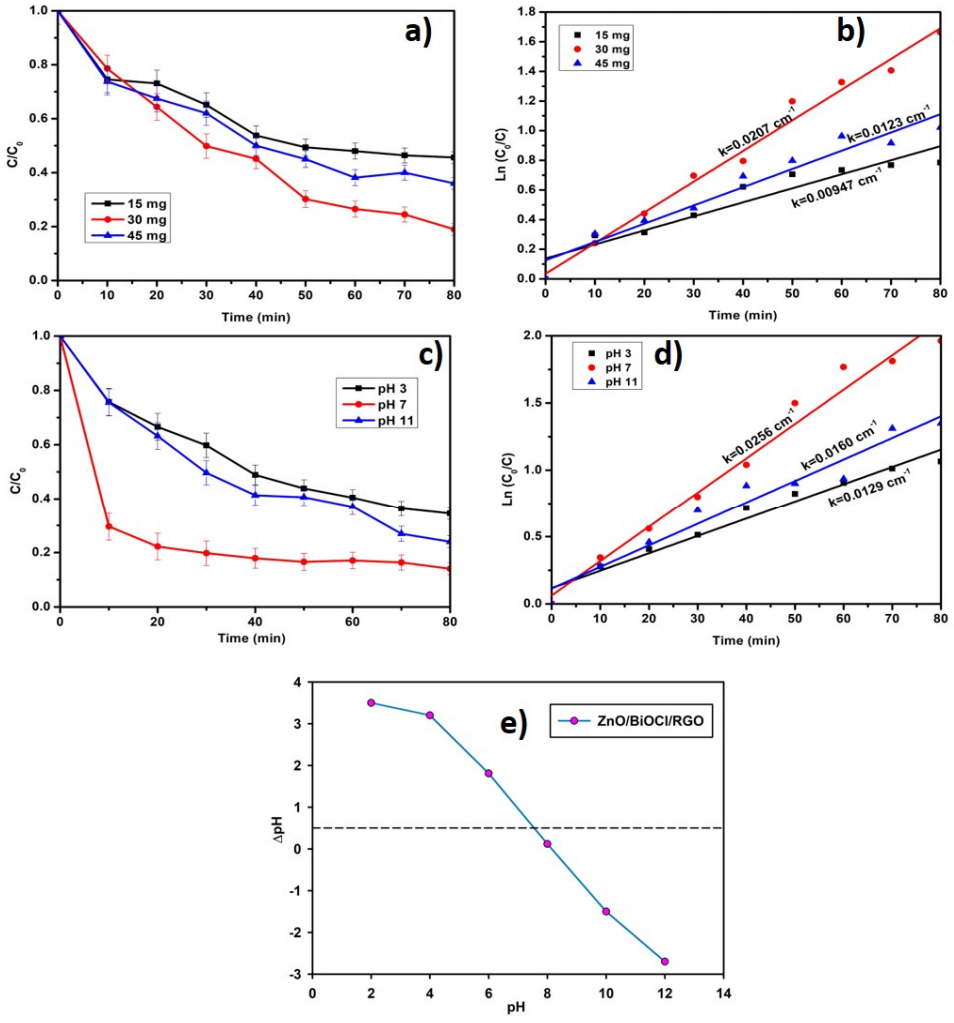

Fig. 11. Visible-light-driven photocatalytic degradation of TC using different dosages and pH using ZnO/BiOCl/RGO catalyst (a and c), Pseudo-first-order kinetic plots of Ln (C_0/Ct) vs time (b and d); and point of zero charge of ZnO/BiOCl/RGO catalyst (e)

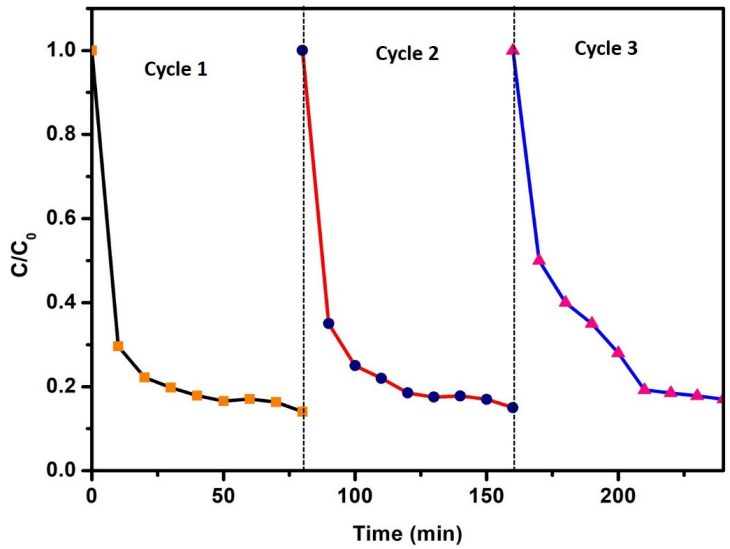

Fig. 12. Reusability study of ZnO/BiOCl/RGO heterostructure for the degradation of TC

Additionally, in the O 1s spectra of ZnO/BiOCl/RGO (Fig. 6f), the peaks at 532.1 and 531.1 eV were ascribed to C-O-Zn and Bi-O. Consequently, the synthesis of the ternary ZnO/BiOCl/RGO heterostructure successfully integrated oxygen-containing RGO into ZnO/BiOCl, as shown by XPS analysis.

3.5. Ultraviolet-visible diffuse reflectance spectroscopy and band gap analysis

Utilizing the UV-visible DRS technique, the light absorption characteristics of the ZnO/BiOCl/RGO heterostructure were measured; the findings are displayed in Fig. 7a. The absorption capability of the photocatalyst is higher in the solar spectrum's visible light portion. At 436 nm wavelength, the band edge absorption value increases both the absorption coefficient and the absorption of visible light. Additionally, the Tauc plot equation is used to compute the optical band gap energies (E_g) [42,43]: $\alpha h\upsilon = A(h\upsilon - E_g)$; where E_g is the band gap energy; h is the Planck constant; α is the absorption coefficient; v is light frequency; A is a proportionality constant.

The calculated E_g value for the ZnO/BiOCl/RGO photocatalyst, based on Tauc plot results (Fig. 7b), is 2.84 eV. Accordingly, the ZnO/BiOCl composite hybridization with RGO may improve the optical absorption characteristics in the visible light spectrum, leading to a superior capacity for photocatalytic degradation.

3.6. Antibacterial potential of ZnO/BiOCl/RGO heterostructure

Fig. 8 and Table 1 show the findings of the antibacterial activity study. In comparison to the control, the synthesized ZnO/BiOCl/RGO showed a notable inhibition zone against *S. aureus* and *E. coli*. The following order of size-dependent antibacterial activity was observed: ZnO/BiOCl/RGO, ZnO/BiOCl, and ZnO, respectively. Their morphology and composition may also be connected to this discrepancy [44]. It was clear that all ZnO heterostructures had the strongest antibacterial action against *S. aureus* at a concentration of 2 mg/mL compared to *E. coli*, most likely due to the different bacterial cell wall compositions [44]. Polar facets on ZnO nanoplates have reportedly demonstrated stronger antibacterial activity. Numerous studies have demonstrated that the action of ZnO is linked to the release of reactive oxygen species (ROS) and zinc ions. Hydrogen peroxide (H_2O_2), hydroxyl radicals (OH^-), superoxide (O_2^-), peroxide (O_2^{2-}), and zinc ions are examples of ROS species that attach to the negative surface of cell membranes, disrupting cells and causing internal cellular substances to leak out, ultimately leading to cell death [45–49]. Moreover, Puttaraju et al demonstrated the antibacterial property of tetragonal non-toxic BiOCl NPs against *S. aureus* and *P. aeruginosa* [50].

In the present work, we were interested in synthesizing nanoparticles and heterostructures with different sizes and observing their composition-dependent antibacterial activity. Among all synthesized samples, ZnO/BiOCl/RGO with a minimum size of 40-55 nm thickness and 150-300 nm width with evenly distributed RGO sheets showed comparatively significant antibacterial activity against both microorganisms. Their small surface area may also facilitate the maximal interaction with microbial cells to volume ratio [51]. Fig. 9 shows the likely mechanism of the antibacterial action.

3.7. Photocatalytic degradation of TC

Fig. 10 shows the photocatalytic degradation effectiveness of ZnO/BiOCl/RGO towards TC. After 80 min of exposure

J Water Environ Nanotechnol, 2026, 11(3): 431-446
10.22090/jwent.2025.2071386.1966

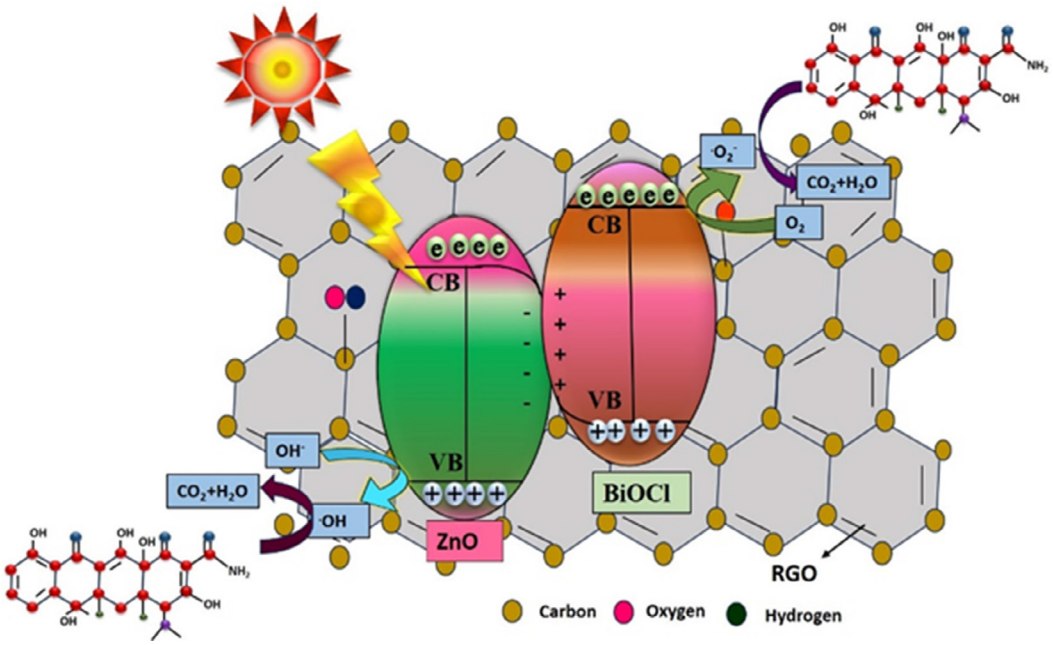

Fig. 13. Proposed photocatalytic mechanism of the prepared ZnO/BiOCl/RGO photocatalyst

to visible light, no discernible changes were seen without the catalyst. According to the figure, the highest TC degradation (85.95%) was seen in 80 min, which may have resulted from the combined action of reduced graphene oxide and BiOCl/ZnO composite [52,53]. Additionally, the Langmuir-Hinshelwood (L-H) model was used to calculate the reaction kinetics [54]; $-\ln(C/C_0) = kt$, where C_0 and C stand for the TC's starting and final concentrations, respectively, and k and t for the rate constant and irradiation duration.

Fig. 10c depicts the pseudo-first-order kinetics of TC degradation, which were supported by the linear relationship of degradation with time, and the rate constant (k) value of ZnO/BiOCl/RGO is 0.0172 min^{-1}, indicating the greater degradation efficacy of the prepared photocatalyst towards the tetracycline pollutant. Furthermore, the comparison of the degradation efficacy of different photocatalysts towards TC antibiotic is tabulated in Table 2.

3.7.1 Effect of dosage

The concentration of the photocatalyst is crucial in the photodegradation process. Generally, reduced photocatalyst concentration diminishes degradation efficiency due to decreased photon absorption. Nonetheless, increasing the photocatalyst concentration enhances the degradation efficiency owing to a greater number of active sites on its surface [25]. The impact of the initial concentration of the synthesized photocatalyst under visible light was examined by varying the ZnO/BiOCl@RGO concentration from 15 mg to 45 mg per 50 mL of 10 mg L^{-1} TC solutions. The results are illustrated in Fig. 12. Fig. 11a illustrates that the photocatalytic degradation efficiency significantly increases at a photocatalyst concentration of 30 mg, then declines with further increase in concentration. This observation may result from increased turbidity in the TC solution when the photocatalyst concentration increases [55]. Consequently, 30 mg is the ideal dosage, demonstrating the highest photocatalytic efficiency under VLI.

Furthermore, the reaction kinetics were determined using the Langmuir-Hinshelwood (L-H) model, given as

$$-\ln\left(\frac{C}{C_0}\right)=kt \quad (1)$$

Where C_0 and C are the initial and final concentrations of the TC; k and t represent the rate constant and irradiation time. From the linear fit (Fig. 11 b), the calculated rate constant values of ZnO/BiOCl/RGO for 15, 30, and 45 mg of catalysts are 0.00947 min^{-1}, 0.0123 min^{-1}, and 0.0207 $min^{-1,}$ respectively.

3.7.2 Effect of pH

The influence of pH on absorption capacity is contingent upon the structure of TC and the functional groups present on the surface of the ZnO/BiOCl/RGO composite. The findings (Fig. 11c) indicate that the elimination of TC is significantly influenced by the pH of the solution. When the pH of TC is less than 3.3, the dimethylammonium group is protonated, resulting in the cationic form of TC. Nonetheless, within the pH range of 3.3 to 7.7, it exists in zwitterionic form, and above a pH of 7.7, TC exists in an anionic state. In acidic conditions,

the surface charge is predominantly positive, but in alkaline conditions, it becomes negatively charged [56]. This aligns with the measurement of the pHZpc of the ZnO/BiOCl/RGO catalyst, which was recorded at 8.11 (Fig. 11e). Under acidic and alkaline conditions, the electrostatic repulsion between TC molecules and the ZnO/BiOCl/RGO catalyst diminishes the adsorption capability. Thus, pH 7 appears to be optimal for efficient TC removal [57]. The determined kinetic rate constants (Fig. 11d) for TC at pH levels of 3, 7, and 11 are 0.0129 min^{-1}, 0.0256 min^{-1}, and 0.0160 min^{-1}, respectively.

3.7.3 Reusability study of synthesized photocatalyst

The photostability and reusability of the ZnO/BiOCl/RGO heterostructure were evaluated by a degradation experiment comprising three cycles. Following each cycle, the photocatalyst was subjected to centrifugation, and residual particles were removed using multiple washes with deionized water and alcohol. The material was subsequently dried in an oven at 70°C for 12 hours to produce a reusable catalyst. Fig. 12 illustrates the deterioration performance, with just a minor reduction after three cyclic runs. The catalyst exhibited 80.0 % degradation efficacy after three cycles, thus confirming the exceptional photostability and reusability of the synthesised photocatalyst.

3.6.1. Plausible Photocatalytic degradation mechanism

Pristine ZnONPs display limited absorption capabilities in the visible part of the solar spectrum because of their broad band gap (3.2 eV). However, its band gap decreases when it is linked with n-type bismuth oxychloride semiconductor, allowing it to absorb visible light from the solar spectrum. However, the agglomeration of nanoparticles in the binary BiOCl/ZnO composite also affects the light absorption capacity. Therefore, the BiOCl/ZnO composite can be immobilized on reduced graphene oxide [58]. The immobilization of the BiOCl/ZnO composite on the RGO surface inhibits electron and hole recombination during photocatalytic activity.

Additionally, the electrons in the CB of ZnO and the holes in the VB of BiOCl create an internal electric field (IEF), which facilitates the migration of the electrons in the CB of BiOCl on the RGO surface [40]. These electrons convert the dissolved oxygen on the RGO surface to superoxide ($O_2^{\bullet-}$) radicals, which oxidize TC into CO_2 and water. Similarly, the holes from the valence band of ZnO efficiently oxidize hydroxyl anion (OH^-) to hydroxyl radicals ($^{\bullet}OH$), which further reduce tetracycline molecules to water and carbon dioxide products. The plausible degradation mechanism using ZnO/BiOCl/RGO heterostructure is represented in Fig. 10.

CONCLUSION

The scarcity of clean and pure water is one of the environmental challenges imposed due to urbanization and industrialization. In addition to managing wastewater, researchers are working very hard to provide clean and safe water. The present study attempts to find a socially and economically viable solution to eliminate TC, a major pollutant of environmental contamination, and to find materials that can stop bacteria from growing. In the present research work, a ZnO/BiOCl/RGO photocatalyst was synthesized by a hydrothermal method, and the catalyst was further utilized for the degradation of the tetracycline antibiotic. Adding RGO enhanced the degradation ability of the ZnO/BiOCl composite as it boosted the charge transfer phenomenon. The RGO material surface offers several active adsorption and degradation sites as it hinders the photoexcited charge carriers (e^- and h^+). ZnO/BiOCl/RGO photocatalyst has a notable degradation efficiency of 85.95% in 80 min. The ZnO/BiOCl/RGO also revealed enhanced antibacterial activity, attributed to improved bacterial cell wall penetration.

In a nutshell, the ZnO/BiOCl/RGO photocatalyst offers a viable method of breaking down hazardous pollutants in wastewater and an affordable solution to clean the environment. This study lays the foundation for further research to improve bactericidal and photocatalytic materials and investigate their uses in various environmental contexts to create sustainable water management solutions and antibacterial applications.

Conflict of Interest
The authors declare no conflict of interest.

Funding
This study was not supported by any funding.

Author's Contributions

Study Conception or Design: VM

Data Acquisition: SM, KK, PB, PH, DH

Data Analysis or Interpretation: SM, PB, PH, DH

Manuscript Drafting: SM

Critical Manuscript Revision: SG, KK, DH, VM

All authors have approved the final manuscript and are responsible for all aspects of the work.

AI Statement
The authors confirm that no AI tools or services were used during the preparation of this work.

Data availability
Data will be made available on request.

REFERENCES

1. Daghrir R, Drogui P. Tetracycline antibiotics in the environment: a review. Environ Chem Lett. 2013;11(3):209-227. https://doi.org/10.1007/s10311-013-0404-8
2. Abbasi Moud A. Polymer based flocculants: Review of water purification applications. J Water Process Eng. 2022;48:102938. https://doi.org/10.1016/j.jwpe.2022.102938

3. Singh NB, Nagpal G, Agrawal S, Rachna. Water purification by using Adsorbents: A Review. Environ Technol Innov. 2018;11:187-240. https://doi.org/10.1016/j.eti.2018.05.006
4. Temesgen G, Lelago A, Assefa E, Admasie A. Evaluation of chlorination efficiency on improving microbiological and physicochemical parameters in water samples available in Sheble Berenta district Amhara region, Ethiopia. Appl Water Sci. 2023;13:120. https://doi.org/10.1007/s13201-023-01922-5
5. Lawrencia D, Chuah LH, Srikhumsuk P, Poh PE. Biodegradation factors and kinetic studies of point-of-use water treatment membrane in soil. Process Saf Environ Prot. 2022;161:392-408. https://doi.org/10.1016/j.psep.2022.03.053
6. Sun H, He F, Choi W. Production of Reactive Oxygen Species by the Reaction of Periodate and Hydroxylamine for Rapid Removal of Organic Pollutants and Waterborne Bacteria. Environ Sci Technol. 2020;54(10):6427-6437. https://doi.org/10.1021/acs.est.0c00817
7. Bhavsar KS, Labhane PK, Murade VD, Dhake RB, Sonawane GH. A photocatalyst: Zinc sulfides nanospheres immobilized on activated carbon for the abatement of aquatic organic pollutants. Inorg Chem Commun. 2021;133:108958. https://doi.org/10.1016/j.inoche.2021.108958
8. Bhavsar KS, Labhane PK, Murade VD, Sonawane GH. Carbon nanofibers (CNf) cocatalyst-integrated CdS nanoflowers photocatalyst for the deterioration of rhodamine B. Inorg Chem Commun. 2024;160:111901. https://doi.org/10.1016/j.inoche.2023.111901
9. Dichayal S, Hase D, Murade R, Deshmukh S, Sillanpää M, Murade V, et al. Synthesis, characterization, and photocatalytic potential of CoFe2O4 nanoparticles immobilized on graphitic carbon nitride. Transit Met Chem. 2025;50(3):1-14. https://doi.org/10.1007/s11243-025-00667-1
10. Murade R, Hase D, Gurav S, Kadam K, Murade V, Aher H. Sol-gel auto combustion synthesis, characterization and enhanced photocatalytic efficiency of NiFe2O4 nanoparticles immobilized on graphitic carbon nitride. J Nanopart Res. 2025;27:303. https://doi.org/10.1007/s11051-025-06500-1
11. Patel S, Hase D, Bhavsar K, Murade V. Green Synthesis of Co3O4/AC Nanocomposite using Bryophyllum pinnatum Leaf Extract for Enhanced Photodegradation of Malachite Green Dye. J Water Environ Nanotechnol. 2025;10(2):141-151.
12. Darandale SV, Hase D, Mane K, Khedkar J, Murade RD, Dichayal SS, et al. Synthesis of Spinel Ferrites and Their Composites: A Comprehensive Review on Synthesis Methods, Characterization Techniques, and Photocatalytic Applications. J Chem Rev. 2025;7(2):216-235.
13. Musmade S, Hase D, Kadam K, Pandhare G, Bhavsar K, Khan MS, et al. Integrating ZnO/BiOCl@rGO Derived S-Scheme Photocatalyst: Characterization and Mechanistic Insight for Environmental Remediation. J Inorg Organomet Polym Mater. 2024;35(2):1008-1023. https://doi.org/10.1007/s10904-024-03389-6
14. Chang JQ, Zhong Y, Hu CH, Luo JL, Wang PG. Study on highly efficient BiOCl/ZnO p-n heterojunction: Synthesis, characterization and visible-light-excited photocatalytic activity. J Mol Struct. 2019;1183:209-216. https://doi.org/10.1016/j.molstruc.2019.01.095
15. Zhang P, Wang T, Chang X, Gong J. Effective Charge Carrier Utilization in Photocatalytic Conversions. Acc Chem Res. 2016;49(5):911-921. https://doi.org/10.1021/acs.accounts.6b00036
16. Zhang Z, Zada A, Cui N, Liu N, Liu M, Yang Y, et al. Synthesis of Ag Loaded ZnO/BiOCl with High Photocatalytic Performance for the Removal of Antibiotic Pollutants. Crystals. 2021;11(8):981. https://doi.org/10.3390/cryst11080981
17. Bhavsar KS, Labhane PK, Dhake RB, Sonawane GH. Crystal structures, morphological, optical, adsorption, kinetic and photocatalytic degradation studies of activated carbon loaded BiOBr nanoplates prepared by solvothermal method. Inorg Chem Commun. 2019;104:134-144. https://doi.org/10.1016/j.inoche.2019.04.002
18. Sánchez-Rodríguez D, Méndez Medrano MG, Remita H, Escobar-Barrios V. Photocatalytic properties of BiOCl-TiO2 composites for phenol photodegradation. J Environ Chem Eng. 2018;6(1):1601-1612. https://doi.org/10.1016/j.jece.2018.01.061
19. Liu X, Xu H, Li D, Zou Z, Xia D. Facile Preparation of BiOCl/ZnO Heterostructure with Oxygen-Rich Vacancies and Its Enhanced Photocatalytic Performance. ChemistrySelect. 2019;4(42):12245-12251. https://doi.org/10.1002/slct.201902964
20. Yang X, Sun S, Cui J, Yang M, Yang Q, Xiao P, et al. One-pot construction of robust BiOCl/ZnO p-n heterojunctions with semi-coherent interfaces toward improving charge separation for photodegradation enhancement. Nanoscale Adv. 2021;3(16):4851-4857. https://doi.org/10.1039/D1NA00396H
21. Mussa Y, Ahmed F, Arsalan M, Alsharaeh E. Two dimensional (2D) reduced graphene oxide (RGO)/hexagonal boron nitride (h-BN) based nanocomposites as anodes for high temperature rechargeable lithium-ion batteries. Sci Rep. 2020;10:1882. https://doi.org/10.1038/s41598-020-58439-z
22. Murade VD, Darandale S, Hase DD. 2D Graphene Oxide and Reduced Graphene Oxide Material for Efficient Photocatalytic Degradation of Wastewater Pollutants: A Comprehensive Review. J Water Environ Nanotechnol. 2025;10(3):267-285.
23. Jahan N, Roy H, Reaz AH, Arshi S, Rahman E, Firoz SH, et al. A comparative study on sorption behavior of graphene oxide and reduced graphene oxide towards methylene blue. Case Stud Chem Environ Eng. 2022;6:100239. https://doi.org/10.1016/j.cscee.2022.100239
24. Mondal A, Prabhakaran A, Gupta S, Subramanian VR. Boosting Photocatalytic Activity Using Reduced Graphene Oxide (RGO)/Semiconductor Nanocomposites: Issues and Future Scope. ACS Omega. 2021;6(13):8734-8743. https://doi.org/10.1021/acsomega.0c06045
25. Hassaan MA, El-Nemr MA, Elkatory MR, Ragab S, Niculescu VC, El Nemr A. Principles of Photocatalysts and Their Different Applications: A Review. Top Curr Chem. 2023;381(6):31. https://doi.org/10.1007/s41061-023-00444-7
26. Choi N, Tang C, Park Y, Du A, Ayoko GA, Hwang Y, et al. Visible-light-driven photocatalytic degradation of tetracycline using citric acid and lemon juice-derived carbon quantum dots incorporated TiO2 nanocomposites. Sep Purif Technol. 2024;350:127836. https://doi.org/10.1016/j.seppur.2024.127836
27. Shan J, Wu X, Li C, Hu J, Zhang Z, Liu H, et al. Photocatalytic degradation of tetracycline hydrochloride by a Fe3O4/g-C3N4/rGO magnetic nanocomposite mechanism: modeling and optimization. Environ Sci Pollut Res. 2023;30(3):8098-8109.

https://doi.org/10.1007/s11356-022-22770-x
28. Mahamuni-Badiger PP, Patil PM, Badiger MV, Patel PR, Thorat-Gadgil BS, Pandit A, et al. Biofilm formation to inhibition: Role of zinc oxide-based nanoparticles. Mater Sci Eng C. 2020;108:110319. https://doi.org/10.1016/j.msec.2019.110319
29. Mahamuni-Badiger PP, Patil PM, Patel PR, Dhanavade MJ, Badiger MV, Marathe YN, et al. Electrospun poly(3-hydroxybutyrate-co-3-hydroxyvalerate)/polyethylene oxide (PEO) microfibers reinforced with ZnO nanocrystals for antibacterial and antibiofilm wound dressing applications. New J Chem. 2020;44(23):9754-9766. https://doi.org/10.1039/D0NJ01384F
30. Asaulyuk T, Saribyekova Y, Semeshko O, Kulish I. Synthesis and Structural Characterization of ZnO Nanoparticles. Her Khmelnytskyi Natl Univ Tech Sci. 2022;311(4):35-41. https://doi.org/10.31891/2307-5732-2022-311-4-35-41
31. Sánchez-Rodríguez D, Jasso-Salcedo AB, Hedin N, Church TL, Aizpuru A, Escobar-Barrios VA. Semiconducting Nanocrystalline Bismuth Oxychloride (BiOCl) for Photocatalytic Reduction of CO2. Catalysts. 2020;10(9):998. https://doi.org/10.3390/catal10090998
32. Gu X, Yan Q, Wei Y, Luo Y, Sun Y, Zhao D, et al. Visible-light-responsive photocatalyst with a microsphere structure: preparation and photocatalytic performance of CQDs@BiOCl. J Mater Sci Mater Electron. 2019;30(17):16321-16336. https://doi.org/10.1007/s10854-019-02003-7
33. Ranjbar-Azad M, Behpour M. Facile in situ co-precipitation synthesis of CuO-NiO/rGO nanocomposite for lithium-ion battery anodes. J Mater Sci Mater Electron. 2021;32(13):18043-18056. https://doi.org/10.1007/s10854-021-06346-y
34. Faniyi IO, Fasakin O, Olofinjana B, Adekunle AS, Oluwasusi TV, Eleruja MA, et al. The comparative analyses of reduced graphene oxide (RGO) prepared via green, mild and chemical approaches. SN Appl Sci. 2019;1(10):1181. https://doi.org/10.1007/s42452-019-1188-7
35. Davarpanah M, Ahmadpour A, Rohani Bastami T. Preparation and characterization of anion exchange resin decorated with magnetite nanoparticles for removal of p-toluic acid from aqueous solution. J Magn Magn Mater. 2015;375:177-183. https://doi.org/10.1016/j.jmmm.2014.09.065
36. Lin W, Yu X, Zhu Y, Zhang Y. Graphene Oxide/BiOCl Nanocomposite Films as Efficient Visible Light Photocatalysts. Front Chem. 2018;6:274. https://doi.org/10.3389/fchem.2018.00274
37. Han Y, Park S, Kim S, Han S, Kim Y, Jeon HS. Enhanced photocatalytic activity of ultrahigh-surface-area TiO2@C nanorod aggregates with hierarchical porosities synthesized from natural ilmenite. J Environ Chem Eng. 2021;9(1):104438. https://doi.org/10.1016/j.jece.2020.104438
38. Sansenya T, Masri N, Chankhanittha T, Senasu T, Piriyanon J, Mukdasai S, et al. Hydrothermal synthesis of ZnO photocatalyst for detoxification of anionic azo dyes and antibiotic. J Phys Chem Solids. 2022;160:110353. https://doi.org/10.1016/j.jpcs.2021.110353
39. Raja A, Son N, Kang M. Construction of visible-light driven Bi2MoO6-rGO-TiO2 photocatalyst for effective ofloxacin degradation. Environ Res. 2021;199:111261. https://doi.org/10.1016/j.envres.2021.111261
40. Moussa H, Girot E, Mozet K, Alem H, Medjahdi G, Schneider R. ZnO rods/reduced graphene oxide composites prepared via a solvothermal reaction for efficient sunlight-driven photocatalysis. Appl Catal B Environ. 2016;185:11-21. https://doi.org/10.1016/j.apcatb.2015.12.007
41. Huang J, Chen W, Yu X, Fu X, Zhu Y, Zhang Y. Fabrication of a ternary BiOCl/CQDs/rGO photocatalyst: The roles of CQDs and rGO in adsorption-photocatalytic removal of ciprofloxacin. Colloids Surf A Physicochem Eng Asp. 2020;597:124758. https://doi.org/10.1016/j.colsurfa.2020.124758
42. Makuła P, Pacia M, Macyk W. How To Correctly Determine the Band Gap Energy of Modified Semiconductor Photocatalysts Based on UV-Vis Spectra. J Phys Chem Lett. 2018;9(23):6814-6817. https://doi.org/10.1021/acs.jpclett.8b02892
43. Chitalkar K, Hase D, Gurav S, Musmade S, Gaikar R, Sillanpää M, et al. Sol-gel Synthesis of Ternary ZnO-Cu2O@AC Nanocomposite: Characterization and Photocatalytic Application for Environmental Remediation. J Inorg Organomet Polym Mater. 2025;35(3):1302-1318. https://doi.org/10.1007/s10904-025-03705-8
44. Mahamuni PP, Patil PM, Dhanavade MJ, Badiger MV, Shadija PG, Lokhande AC, et al. Synthesis and characterization of zinc oxide nanoparticles by using polyol chemistry for their antimicrobial and antibiofilm activity. Biochem Biophys Rep. 2019;17:71-80. https://doi.org/10.1016/j.bbrep.2018.11.007
45. Mahamuni-Badiger P, Patel PR, Patil PM, Gurav R, Hwang S, Dhanavade MJ. Bioremediation of Industrial Wastewater: An Overview with Recent Developments. In: Advanced and Innovative Approaches for Environmental Biotechnology in Industrial Wastewater Treatment. Singapore: Springer Nature; 2023. p. 333-359. https://doi.org/10.1007/978-981-99-2598-8_15
46. Yue L, Wang M, Khan IM, Niazi S, Wang B, Ma X, et al. Preparation and characterization of chitosan oligosaccharide derivatives containing cinnamyl moieties with enhanced antibacterial activities. LWT. 2021;147:111663. https://doi.org/10.1016/j.lwt.2021.111663
47. Sathiyaseelan A, Vishven Naveen K, Zhang X, Han K, Wang MH. Research progress on chitosan-zinc oxide nanocomposites fabrication, characterization, biomedical and environmental applications. Coord Chem Rev. 2023;496:215398. https://doi.org/10.1016/j.ccr.2023.215398
48. Gad S, Murade V, Nadaf S, Hase D, Salve P, Kalaskar M, et al. Experimental exploration of QbD employed bio-inspired chitosan/zinc oxide nanocomposites for water remediation. Int J Biol Macromol. 2025;322:146951. https://doi.org/10.1016/j.ijbiomac.2025.146951
49. Ahmed R, Tariq M, Ali I, Asghar R, Noorunnisa Khanam P, Augustine R, et al. Novel electrospun chitosan/polyvinyl alcohol/zinc oxide nanofibrous mats with antibacterial and antioxidant properties for diabetic wound healing. Int J Biol Macromol. 2018;120:385-393. https://doi.org/10.1016/j.ijbiomac.2018.08.057
50. Puttaraju TD, Manjunatha M, Nagaraju G, Lingaraju K, Naika HR, Manjula MV, et al. The evaluation of various biological properties for bismuth oxychloride nanoparticles (BiOCl NPs). Inorg Chem Commun. 2022;144:109850. https://doi.org/10.1016/j.inoche.2022.109850
51. Dorazehi J, Farrokhi M, Bastami TR, Meshkat Z, Mahmoudi V, Tanzadehpanah H, et al. Exploration of the antiviral

and antibacterial efficacy of hydrozincite/graphene oxide nanocomposites: Molecular docking and in vitro investigations. J Environ Chem Eng. 2025;13(6):118940. https://doi.org/10.1016/j.jece.2025.118940

52. Asgharian M, Mehdipourghazi M, Khoshandam B, Keramati N. Experimental design and RSM modeling of tetracycline photocatalytic degradation using rGO/ZnO/Cu. Desalin Water Treat. 2020;195:177-185. https://doi.org/10.5004/dwt.2020.25878
53. Gang R, Xu L, Xia Y, Zhang L, Wang S, Li R. Facile One-step Production of 2D/2D ZnO/rGO Nanocomposites under Microwave Irradiation for Photocatalytic Removal of Tetracycline. ACS Omega. 2021;6(5):3831-3839. https://doi.org/10.1021/acsomega.0c05559
54. Sun P, Zhang J, Liu W, Wang Q, Cao W. Modification to L-H Kinetics Model and Its Application in the Investigation on Photodegradation of Gaseous Benzene by Nitrogen-Doped TiO2. Catalysts. 2018;8(8):326. https://doi.org/10.3390/catal8080326
55. Subasi BS, Hayri-Senel T, Kahraman E, Sezer S, Nasun-Saygili G, Erdol-Aydin N. Photocatalytic degradation of tetracycline from aqueous solution with graphene oxide and hydroxyapatite composites. Sci Rep. 2025;15:25894. https://doi.org/10.1038/s41598-025-11502-z
56. Jannat Abadi MH, Nouri SMM, Zhiani R, Heydarzadeh HD, Motavalizadehkakhky A. Removal of tetracycline from aqueous solution using Fe-doped zeolite. Int J Ind Chem. 2019;10(4):291-300. https://doi.org/10.1007/s40090-019-0191-6
57. Davarpanah M, Ahmadpour A, Rohani-Bastami T, Dabir H. Synthesis and application of diethanolamine-functionalized polystyrene as a new sorbent for the removal of p-toluenesulfonic acid from aqueous solution. J Ind Eng Chem. 2015;30:281-288. https://doi.org/10.1016/j.jiec.2015.05.034
58. Qin Y, Sun Z, Zhao W, Liu Z, Ni D, Ma Z. Improved photocatalytic properties of ZnS/RGO nanocomposites prepared with GO solution in degrading methyl orange. Nano-Struct Nano-Objects. 2017;10:176-181. https://doi.org/10.1016/j.nanoso.2017.05.005
59. Yan M, Wu Y, Liu X. Photocatalytic nanocomposite membranes for high-efficiency degradation of tetracycline under visible light: An imitated core-shell Au-TiO2-based design. J Alloys Compd. 2021;855:157548. https://doi.org/10.1016/j.jallcom.2020.157548
60. Wu S, Li X, Tian Y, Lin Y, Hu YH. Excellent photocatalytic degradation of tetracycline over black anatase-TiO2 under visible light. Chem Eng J. 2021;406:126747. https://doi.org/10.1016/j.cej.2020.126747
61. Liu R, Zhang X, Han X, Sun Y, Jin S, Liu R. Photocatalytic degradation of tetracycline with Fe3O4/g-C3N4/TiO2 catalyst under visible light. Carbon Lett. 2024;34(1):75-83. https://doi.org/10.1007/s42823-023-00661-6